JPhys Materials

PURPOSE-LED PUBLISHING™

PAPER • OPEN ACCESS

Mapping the magnetocaloric effect at the microscale on a ferromagnetic shape memory alloy with infrared thermography

To cite this article: Maria J Pereira *et al* 2023 *J. Phys. Mater.* **6** 024002

IOP Publishing J. Phys. Mater. 6 (2023) 024002 https://doi.org/10.1088/2515-7639/acc13b

Journal of Physics: Materials

OPEN ACCESS

RECEIVED
31 October 2022

REVISED
6 February 2023

ACCEPTED FOR PUBLICATION
3 March 2023

PUBLISHED
28 March 2023

PAPER

Mapping the magnetocaloric effect at the microscale on a ferromagnetic shape memory alloy with infrared thermography

Maria J Pereira[1,*], **Tiago Santos**[1,2,3], **Rafael Correia**[1], **João S Amaral**[1], **Vitor S Amaral**[1], **Simone Fabbrici**[4] **and Franca Albertini**[4]

[1] CICECO—Aveiro Institute of Materials and Physics Department, University of Aveiro, Aveiro, Portugal
[2] TEMA—Center for Mechanical Technology and Automation, University of Aveiro, Aveiro, Portugal
[3] Center for Rapid and Sustainable Product Development (CDRSP), Polytechnic of Leiria, Marinha Grande, Portugal
[4] Institute of Materials for Electronics and Magnetism (IMEM), National Research Council (CNR), Parma, Italy
[*] Author to whom any correspondence should be addressed.

E-mail: mariasapereira@ua.pt

Keywords: magnetocalorics, heat management, infrared thermography, ferromagnetic shape memory

Abstract

An innovative study of the magnetocaloric effect (MCE) was performed by mapping the effect based on direct measurements of the temperature change during magnetic field cycles with microscopic resolution (85 μm) on a Co-doped Ni–Mn–Ga bulk sample using infrared thermography on the whole sample. The MCE maps were constructed for different sample temperatures (T_{sample}), cycling both on heating (from 272.8 K up to T_{sample}, with $T_{sample} \leqslant 327.0$ K) and on cooling (from 340.0 K down to T_{sample}, with $T_{sample} \geqslant 266.8$ K), cycling a 1.2 T magnetic field at each T_{sample} value. The MCE maps were calculated to evaluate the amplitude of the effect at the microscale for all T_{sample} values. This allows to analyze the contribution of each micrometric portion of the sample to the spatially heterogeneous behavior that was found. Significant differences of the MCE on heating and cooling are present associated to inhomogeneity dynamics, mostly near the structural transformation. The amplitude of the MCE and its inhomogeneity are both much more pronounced on the heating process. On the cooling process the effect behaves quite homogeneously since the structural transformation already occurred during the cooling to reach T_{sample}. The behavior of the MCE at selected map coordinates was scrutinized, revealing significant differences amongst sample locations. Moreover, the extreme amplitudes of MCE registered for diverse micro-regions occur at different temperatures, suggesting that the structural transformation occurs at varying temperatures and with different magnitudes. The study innovates by constructing MCE maps to evaluate minority behaviors in the MCE in contrast with the average behavior of the effect. This study displays the capability to discriminate the behavior of the transformation at the microscale.

1. Introduction

Heat transfer management is critical for technological development and research. Understanding thermophysical phenomena is paramount for proper thermal behavior exploration and performance control of modern devices. The existing drive to further reduce the dimensions of devices and applications leads to contemplating such phenomena at reduced scales with increased interest. The dimensional compactation allowed by caloric-centered technologies is an enormous advantage in this field and turns the pursuit of studies of caloric effects at the microscale relevant and alluring [1, 2]. The magnetocaloric effect (MCE) is an insurmountable topic in the context of new creative solutions for heat management. While its main application is in magnetic refrigeration as a friendlier alternative to the vapor compression-based

refrigeration devices, the effect has also been applied in the medical field, for instance in cancer therapy hyperthermia applications and targeted drug delivery [2, 3].

Direct measurements of the MCE have been performed with different techniques [4–6]. A contactless infrared (IR) sensor measured the average adiabatic temperature change (ΔT) on a thin (27 μm) gadolinium sample under a 1.75 T magnetic field in a temperature range between 270 K and 320 K [7]. The obtained results were congruent with data obtained by in-field differential scanning calorimetry measurements, with a maximum of $\Delta T \sim 4$ K at ∼293 K. An IR fiber optical sensor was used on a fast response temperature probe to directly measure the MCE in pulsed magnetic fields for gadolinium near the Curie temperature. A temperature variation of 21.3 K was registered under a magnetic field of 12.7 T. The inverse MCE was observed for a $Fe_{48}Rh_{52}$ sample at the initial temperature of 305.1 K. The measured adiabatic change in temperature under a magnetic field of 8.5 T was −4.5 K [8]. IR thermography was utilized to enable systematic direct measurements of the MCE in gadolinium [9, 10]. At a temperature of 300.5 ± 0.5 K, the sample experienced a temperature change of 1.84 ± 0.11 K under a magnetic field of 1.0 T [9]. Spatially resolved measurements of the MCE took place on a plate of gadolinium using IR thermography and were compared with the results obtained with a numerical model [10]. High-throughput systems have been implemented to perform direct measurements of the MCE with IR thermography on a series of $La_{0.7}Ce_{0.3}Fe_{11.65-x}Mn_xSi_{1.35}$ ($x = 0.07, 0.09, 0.13, 0.15, 0.19$) samples simultaneously. The evolution of the effect during magnetic field cycling (between 0 and 1.3 T) was reported, with an adiabatic change in temperature of 2.12 K after the first cycle [11]. There are several studies contemplating direct measurements of the MCE on Heusler alloys. These alloys, also known as ferromagnetic shape memory alloys (FSMAs), suffer a structural transformation called the martensitic transformation. The MCE was directly measured in a $Ni_{50}Mn_{35}In_{15}$ Heusler alloy in pulsed magnetic fields. The results for 6 T are compared with data obtained from heat-capacity experiments. A saturation of the inverse MCE is observed which is related to the martensitic transition, with a maximum adiabatic temperature change of −7 K at 250 K. The conventional MCE occurs in the vicinity of the ferromagnetic transition [12]. The thermo-optical mirage effect, a contactless temperature measuring technique, evaluated the MCE in micrometric-thick ribbons of Ni–Mn–In–Sn Heusler alloys at the Curie transition under a 1.1 T pulsed magnetic field. The maximum temperature change observed was ∼2 K [13]. IR thermography has been applied to perform direct measurements of the MCE in Ni–Mn-based Heusler alloys. Conventional and inverse MCE were reported in the Ni–Mn–Si–In and Ni–Mn–Co–Sb systems. For these systems, changes in temperature associated with the inverse MCE were found to be smaller than the ones exhibited in the manifestation of the conventional MCE effect [14]. Previous work showed that direct measurements of the MCE at the microscale could be obtained with IR thermography [15]. Bulk Co-doped Ni–Mn–Ga (NMG) was used for this purpose. Strong spatial inhomogeneity of the MCE at the microscopic scale around the reverse martensitic transformation was reported [15]. NMG is one of the most well-known systems of the Ni–Mn-based Heusler alloys. MCE is intensified when the material reaches a temperature in the vicinity of the martensitic transformation temperature (T_M). Differences in the magnetizations of the structural phases involved in the transformation are responsible for the increase in the MCE. When Co is added to the NMG system, the dominant phase in terms of magnetization is reversed in relation to the NMG parent phase [16, 17]. In the latter, an applied external magnetic field will raise the temperature of the sample, originating the direct MCE, while in the former, it will lower the temperature of the sample, which manifests as the inverse MCE, like our sample. The present study aims to extend the previous work by constructing maps of the calculated MCE at the microscale and quantitatively exploring the inhomogeneous behavior of the effect. These maps constitute a key development since they are a built representation of the relative contribution of each microscopic portion of the sample to the MCE. A dynamic representation of the temperature dependence of the MCE is made available in video form [18, 19]. The produced illustrations of the spatial heterogeneities of the MCE throughout the whole sample provide a visually accessible way to discriminate and analyze minority behaviors of the MCE for all considered temperatures, both in heating and cooling.

2. Method

The sample used in this study is a 7 × 4 mm bulk $Ni_{44\pm4}Co_{6\pm1}Mn_{27\pm2}Ga_{23\pm2}$ composite. The composition was provided by energy-dispersive x-ray spectroscopy (EDS), giving an average, with variation in sample surface below experimental uncertainty.

Magnetization measurements as a function of temperature $M(T)$ and the magnetic field $M(H)$ were performed with a Quantum Design MPMS3 SQUID-VSM using magnetic fields from -7 T to 7 T and temperatures ranging between 2 and 400 K. $M(T)$ measurements in the distinct cooling and heating cycles show that the reverse and direct martensitic transformations take place at around 297 K and 288 K, respectively [15].

For the study of the MCE, the (quasi)adiabatic variation in temperature of the sample was measured, when a magnetic field was applied. The experimental setup consisted in mounting the sample on a Peltier element employed to vary the sample's temperature and attaching a thermocouple to the sample to measure said temperature. This ensemble was positioned so that NdFeB permanent magnets in a Halbach geometry could be automatically moved back and forth to apply to and remove from the sample a 1.2 T a magnetic field. The assembly of NdFeB permanent magnets of grade N45 in a Halbach geometry produced the magnetic field. An actuator speeded up the Halbach towards the sample until a constant speed of about 0.5 m s^{-1} was reached within 5 ms. When the Halbach neared the sample, the actuator reduced its speed to zero, also within 5 ms. The quick magnetic field change ensured quasi-adiabatic conditions for the temperature change. The IR camera was a FLIR SC5600-M, with response spectral interval of 2.5 μm to 5.1 μm, 640 $\times$ 512 pixel and 0.02 K resolution, temperature measurement accuracy of $\pm$1 K or $\pm$1% and temperature calibration ranging from 253 K to 3273 K. The 25 Hz frame rate used was considered appropriate to follow the fast quasi-adiabatic temperature change. In this study, a pixel of information recorded by the camera equates to an area of 85 $\times$ 85 μm^2. Further detail on this setup and equipment used is provided elsewhere [15].

For the IR camera measurements of the temperature of the sample's surface, two procedures, A and B, were followed: procedure B for the magnetic field cycling and procedure A for the thermal cycling (to adjust the stage temperature of the sample, T_{sample}). The magnetic field cycling consisted in applying and removing several times a 1.2 T magnetic field to and from the sample while the sample temperature is imaged with the IR camera [15]. Procedure A (thermal cycling) ensured that each measurement (procedure B, field cycling for MCE) took place at T_{sample} after either previous cooling or heating of the sample. The heating process of procedure A consists of cooling down to a fixed minimum temperature (272.8 K) and heating up to T_{sample}. For the cooling process, procedure A ensured that each measurement took place at T_{sample} after heating up to a fixed maximum temperature (340.0 K) and cooling down to T_{sample}. This combination of procedures guarantees that each measurement (B) at a particular T_{sample} is independent of the others [15]. T_{sample} values ranged from 272.8 K up to 327.0 K on heating and on cooling from 323.3 K down to 266.8 K.

Maps of the MCE were built using MATLAB to perform the systematic handling of the data concerning temperature variation for each pixel, at each instant. The presented maps feature the whole sample, for all considered T_{sample} values, both on heating and cooling.

Figure 1 shows a photograph of the sample assembled on the Peltier (top) and the corresponding image provided by the IR camera (bottom) when the sample was set at a temperature of 301.1 K and no magnetic field was applied.

The IR camera measured the sample's surface temperature which stemmed from the effect of the power supplied by the Peltier element and the MCE effect, if present.

3. Results and discussion

As the IR camera measures and records information for each image pixel, micrometer sized areas at the whole sample surface are independently measured. Figure 2(a) represents two areas of the sample selected for global analysis: a blue line-encircled wider area (represented as 1 in figure 1) and a yellow line-encircled smaller area contained within the previous one (represented as 2 in figure 1), when $T_{sample} = 300.0$ K. Figure 2(b) plots temperature data provided by the measurements performed by the IR camera over 23 s, while the magnetic field was applied and removed twice from the sample. The different curves shown correspond to the minimum, maximum and mean temperature values registered in individual pixels within areas 1 and 2 (1 minimum, 1 maximum and 1 mean, and 2 minimum, 2 maximum and 2 mean, respectively). As can be seen, areas 1 and 2 did not display significant differences in mean temperature, which was also the case for the other T_{sample} values considered in this study.

The MCE is characterized by the direct measurement of the temperature change ΔT under magnetic field change. Figure 3 shows the difference in average temperature of the whole sample surface after and before the magnetic field was applied for the first time to the sample at different values of T_{sample}, both in

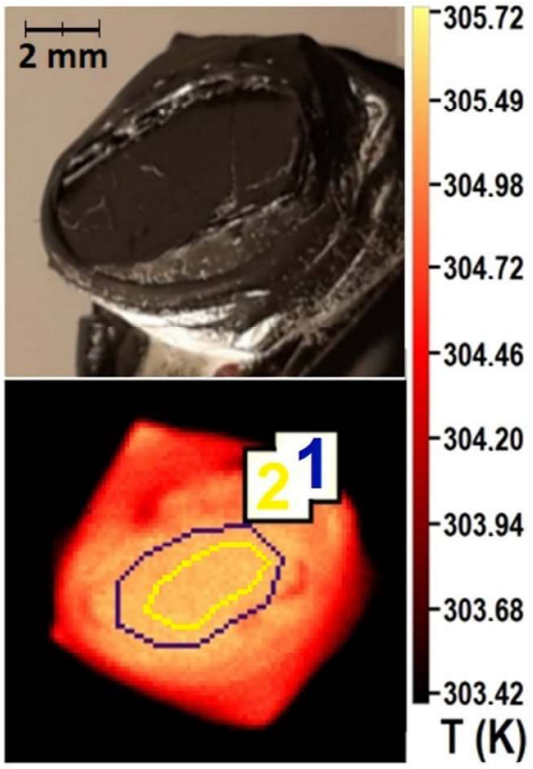

Figure 1. Photograph of the sample when mounted on the Peltier (top) and image provided by the IR camera when the sample was at 301.1 K and no magnetic field applied (bottom). The two areas analyzed are indicated.

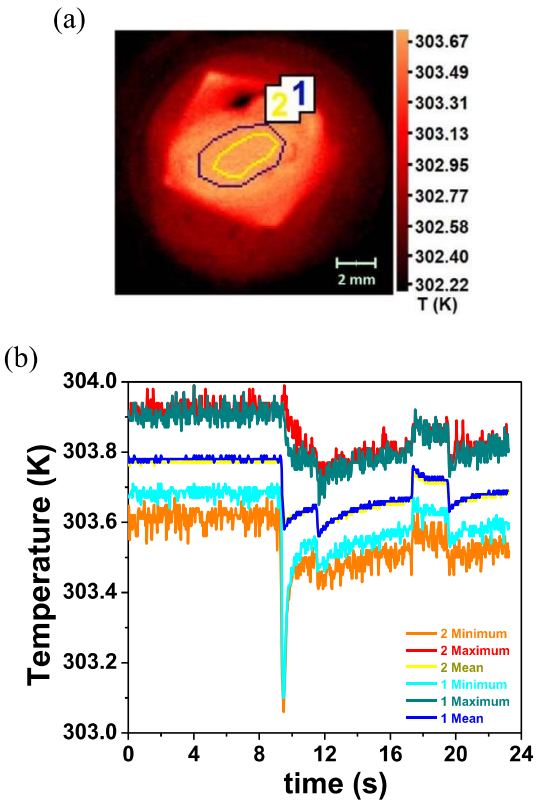

Figure 2. (a) Infrared image of the sample provided by the IR camera when $T_{\text{sample}} = 300.0$ K. (b) Extreme and mean temperature data for areas 1 and 2, provided by the IR camera as a function of time when $T_{\text{sample}} = 300.0$ K during two magnetic field cycles.

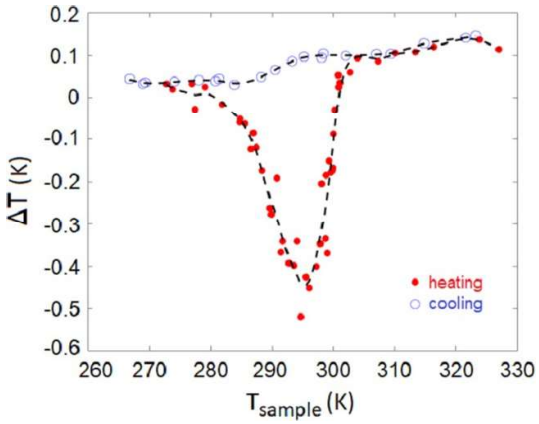

Figure 3. Average temperature change of the sample surface following magnetic field application at different temperatures in heating and cooling. Dashed lines are guides to the eye.

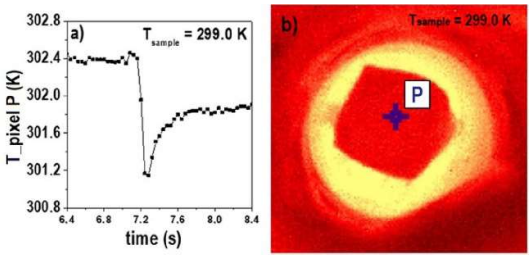

Figure 4. (a) Temperature data provided by the IR camera as a function of time for pixel P when $T_{\text{sample}} = 299.0$ K; (b) Location of pixel P on the sample (cross).

heating and cooling. The data were collected as described in the previous section. Details on the calculation of the difference in average temperature are presented elsewhere [15].

The different trends for average temperature changes observed in the heating and cooling procedures across the magnetostructural transition agree with reports on similar FSMAs with the inverse MCE, using conventional thermocouple methods [20].

Figure 4 shows the time dependence of the temperature for one particular pixel (P) when the magnetic field is first applied to the sample ($T_{\text{sample}} = 299.0$ K). For simplicity, we designate as ΔT the difference in temperature after and before the magnetic field was applied to the sample. This plot shows that we can calculate ΔT and study the behavior of the MCE for any chosen pixel. ΔT is calculated by taking the lowest/highest temperature registered right after the sudden change in temperature and the highest/lowest temperature registered just prior to said change, when in the presence of the direct/reverse MCE [15].

MCE maps were constructed using MATLAB to perform a systematic calculation of ΔT for each pixel, following the application of the magnetic field to the sample for the first time.

Figures 5(a)–(e) and 6(a)–(c) depict, on heating and cooling, respectively, the MCE maps across the evaluated pixels, which span nearly the whole sample surface. Maps for all assessed T_{sample} values were executed. The *x*–*y* scale is presented in arbitrary units (a.u.) resulting from pixel counting, but with a direct correspondence, as in both scales 1 a.u. equals 0.95 mm. The representation of the MCE value at each pixel uses a color scale for immediate visual effect. We use different map color scales for the heating (figure 5) and cooling (figures 6) processes due to significant differences in amplitude of temperature variation between both processes. However, they are the same within each process. In every map a white and a black cross signal the location (pixel) for the minimum and maximum ΔT values, respectively. A few of them will be analyzed in detail later in this section. To enhance the dynamic aspects of the temperature dependence of the MCE, videos were produced collecting all maps on heating [18] and cooling [19].

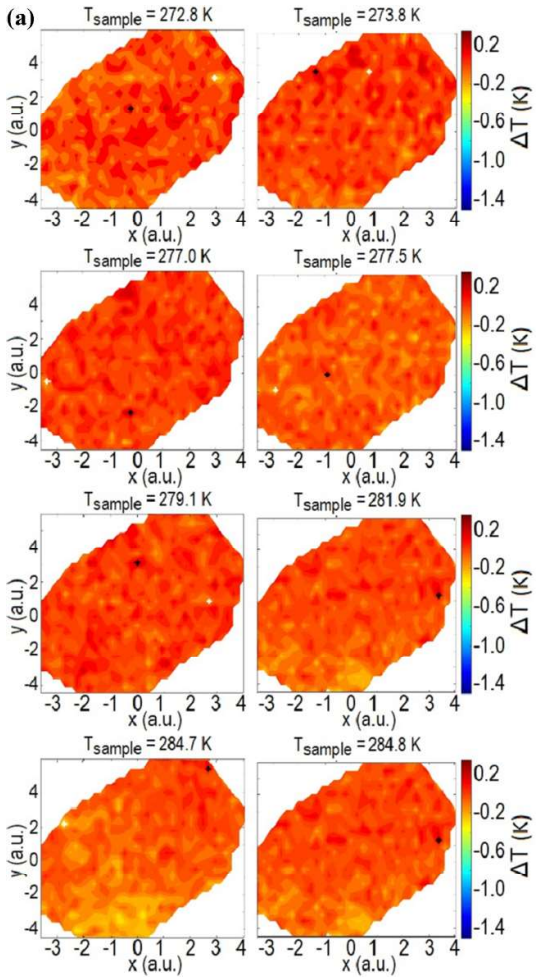

Figure 5. (a) Maps of the MCE amplitude calculated for temperatures between 272.8 K and 284.8 K, while the sample is in the heating process (video available [18]). (b) Maps of the MCE amplitude calculated for temperatures between 285.6 K and 293.6 K, while the sample is in the heating process (video available [18]). (c) Maps of the MCE amplitude calculated for temperatures between 294.1 K and 299.6 K, while the sample is in the heating process (video available [18]). (d) Maps of the MCE amplitude calculated for temperatures between 299.9 K and 313.4 K, while the sample is in the heating process (video available [18]). (e) Maps of the MCE amplitude calculated for temperatures between 316.4 K and 327.0 K, while the sample is in the heating process (video available [18]).

These MCE maps and their collection in video unequivocally show strong spatial inhomogeneity at the microscale and its temperature dependence on the heating process. This is not the case for the cooling process, where the effect occurs in a more homogeneous way.

In figure 5, one can clearly find evidence of the spatial inhomogeneity of the MCE on heating by observing the contrasting behavior between the lower left (characterized by negative x and y coordinates) and the upper right portions of the sample (characterized by positive x and y coordinates). The more intense ΔT values manifest on the lower left portion of the sample for lower T_{sample} values and for higher T_{sample} values on the upper right portion of the sample. Furthermore, the ΔT intensity is more accentuated in the upper right portion.

These overall features can be further analyzed using a particular pixel analysis of its MCE behavior. For pixel selection we designated three T_{sample} values of interest, all belonging to the heating process: 277.0 K (well before T_M), 298.7 K (within the transformation) and 316.4 K (significantly higher than T_M). For each of these T_{sample} values, we identified the particular pixels where the ΔTs resulting from the MCE are maximum (highest positive value or negative value with lowest modulus) and minimum (lowest positive value or negative value with highest modulus). We have thus obtained six distinct locations on the sample surface (figure 7). Their ΔT vs T_{sample} behavior was plotted on heating (figures 8 and 9) and cooling (figures 10 and 11). On heating we find that, for each pixel, there is a temperature where ΔT amplitude is more intense, signaling a negative bump or peak. These extrema occur at temperatures T_{peak} from about

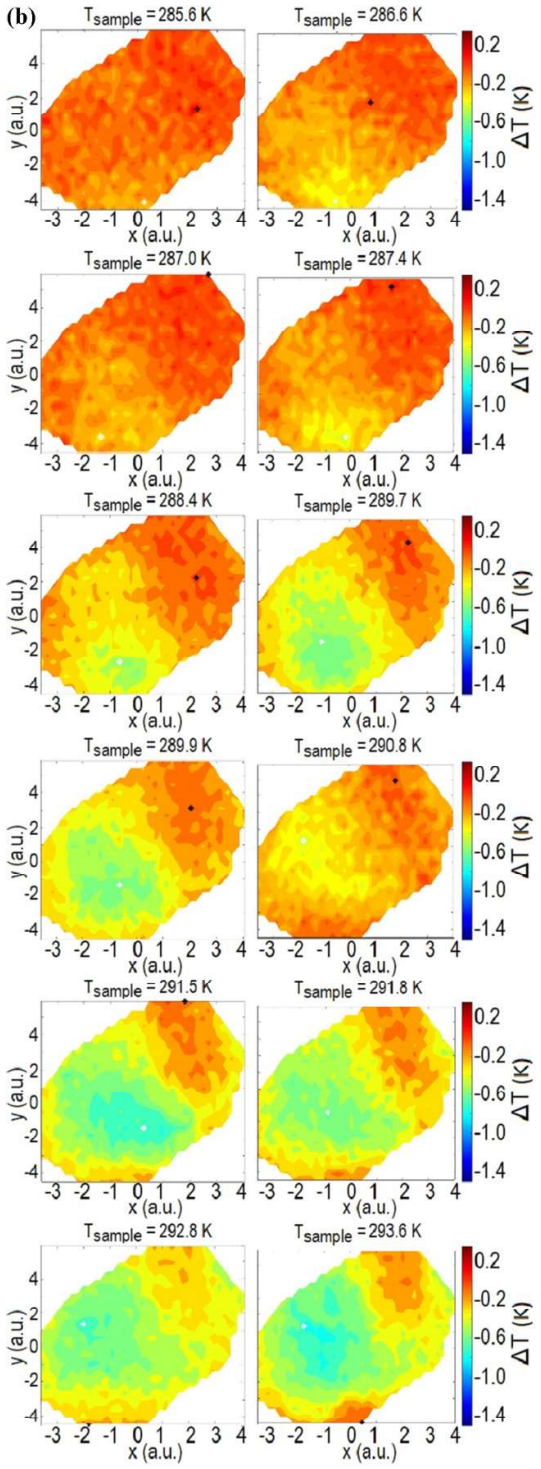

Figure 5. (Continued.)

289 K to 298 K, that indicate the structural transformation triggered by the magnetic field. The pixels with lower T_{peak} values present a smaller ΔT amplitude. At higher temperatures, well in the austenitic phase, when ΔT is positive, the differences between the selected pixels are not relevant. On the other hand, the corresponding cooling curves do not display significative differences across the considered temperature range, which is consistent with the homogeneity of the maps of the cooling process (figures 6(a)–(c)).

To give an overall appreciation of the MCE ΔT inhomogeneity, figures 12(a) and (c) show, for cooling and heating, respectively, the plot of the difference between the maximum and minimum ΔT values (ΔT_{max}

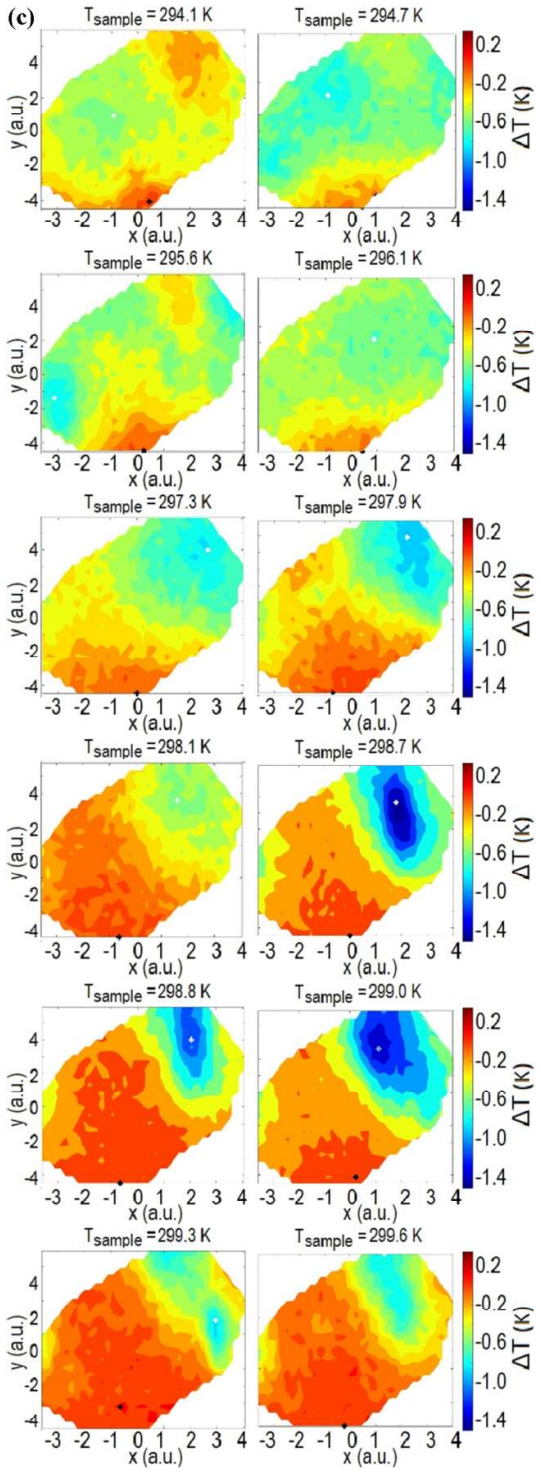

Figure 5. (Continued.)

and ΔT_{min}, respectively) for each T_{sample} value. It must be stressed that the (pixel) locations generally vary from one T_{sample} value to another. For comparison, the difference in average temperature of the sample surface in the same conditions is provided. On cooling, we see that ΔT_{max} values generally increase as T_{sample} values decrease. This behavior is the opposite from the one observed for the average (figure 3). ΔT_{min} values increase when cooling begins, but generally decrease approximately below 315 K as T_{sample} values decrease, which is more similar to the behavior of the average, although the decrease for lower values of T_{sample} is more accentuated for ΔT_{min} values. This leads to an increasing spread of the measured values of ΔT. On heating,

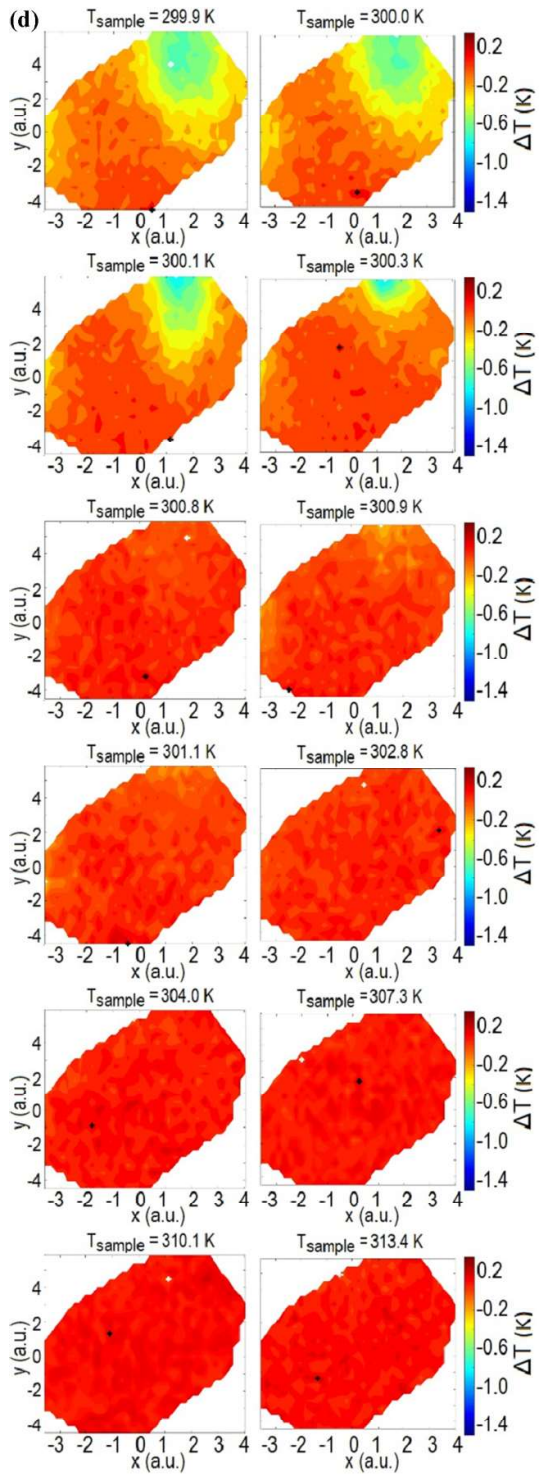

Figure 5. (Continued.)

both ΔT_{max} and ΔT_{min} exhibit behaviors similar to the average, although, as on cooling, variations are more dramatic for ΔT_{min} values.

The difference between the maximum and minimum values of the MCE (ΔT_{max}–ΔT_{min}), on both heating and cooling processes, is plotted in figure 13. The cooling plot is characterized by the absence of dramatic changes, which is to be expected from the behaviors described in the previous paragraphs, increasing with decreasing temperatures. The heating plot shows higher values of the difference compared to the cooling process in the interval 285 K until 300 K, with the most dramatic change occurring just below T_{sample} reaches 300 K.

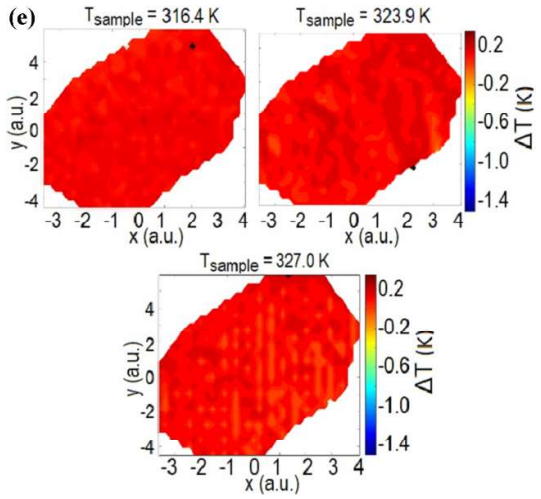

Figure 5. (Continued.)

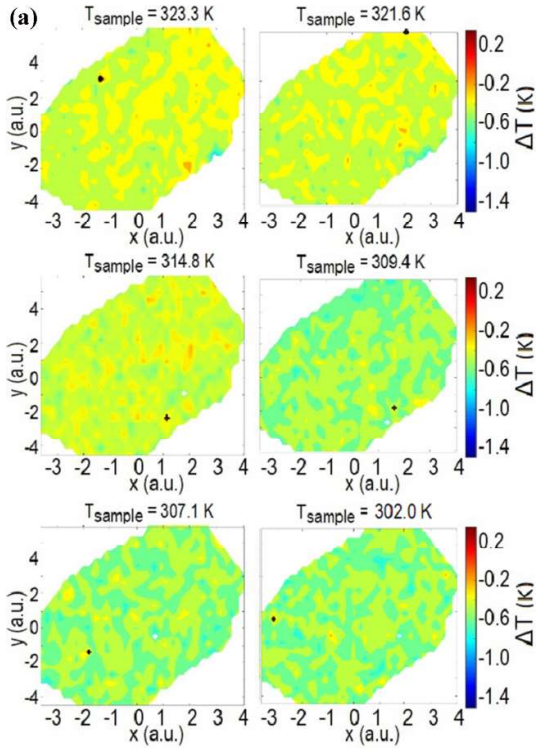

Figure 6. (a) Maps of the MCE amplitude calculated for temperatures between 323.3 K and 302.0 K, while the sample is in the cooling process (video available [19]). (b) Maps of the MCE amplitude calculated for temperatures between 298.4 K and 269.4 K, while the sample is in the cooling process (video available [19]). (c) Maps of the MCE amplitude calculated for temperatures between 269.0 K and 266.8 K, while the sample is in the cooling process (video available [19]).

The chemical composition of the sample was evaluated by EDS in a large collection of spot and the results are homogeneous within experimental uncertainty (typically 2%). This dismissed compositional heterogeneity as a plausible cause for the observed MCE behavior. Such inhomogeneity in the MCE behavior is likely to arise from differences in local stress in the sample's microstructure. The synthesis process (arc melting) may play a role in the local stresses of the sample microstructure. It provides a polycrystalline sample that may show a preferential orientation of the grains shape due to strong temperature gradients occurring during the free cooling. The samples are then heat treated and quenched. Heat treating at high

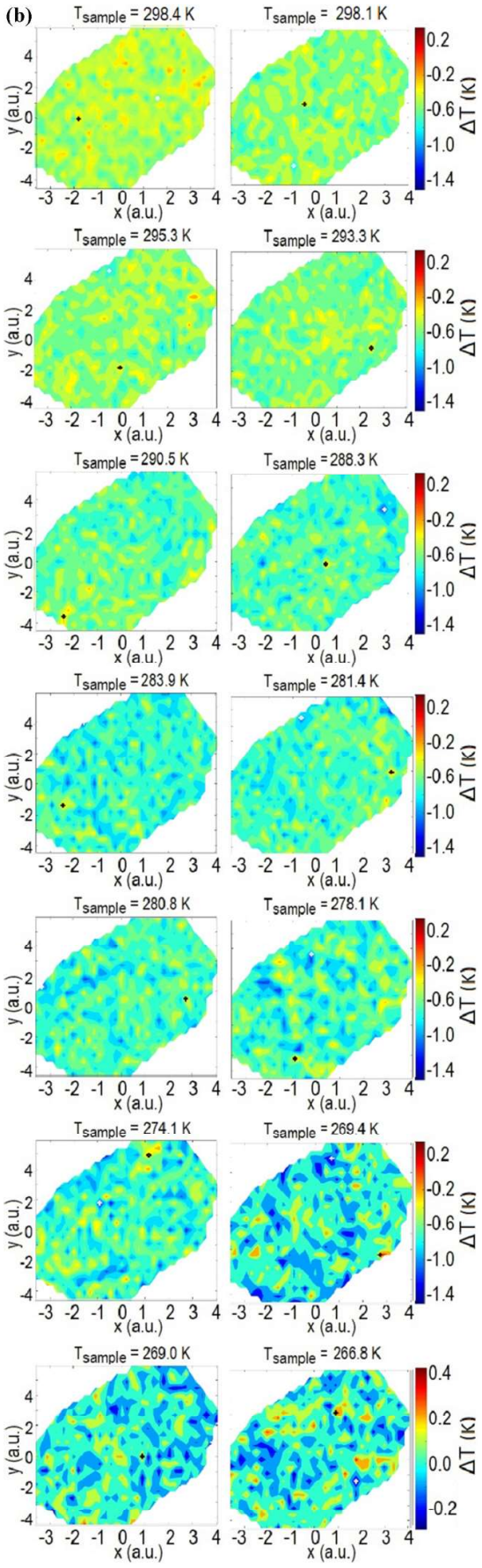

Figure 6. (Continued.)

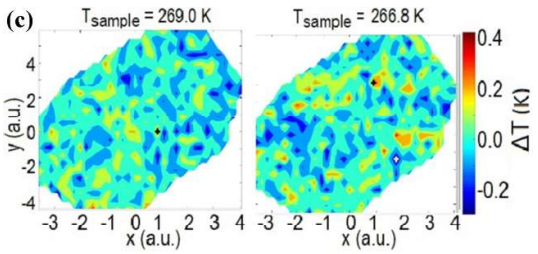

Figure 6. (Continued.)

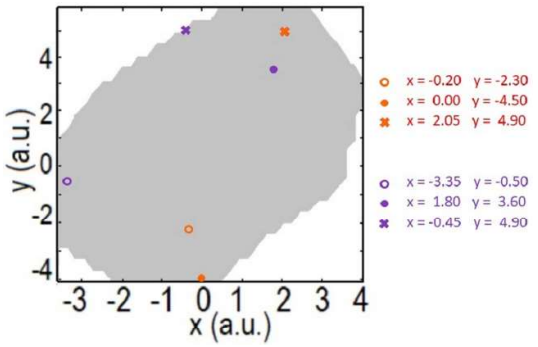

Figure 7. Map coordinates and locations of the pixels where the measured MCE ΔTs at $T = 277.0$ K (open circle), $T = 298.7$ K (full circle) and $T = 316.4$ K (cross) are maximum (orange) and minimum (purple).

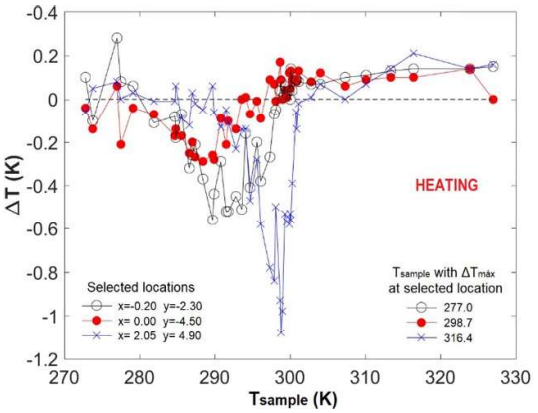

Figure 8. ΔT vs T_{sample} on heating for selected locations of the sample surface. The locations were determined by selecting three T_{sample} values of interest and finding the map coordinates for which the maximum value of ΔT occurred.

temperatures improves homogeneity and impacts the grain growth. However, the final water quenching introduces a lot of stress. There are post synthesis additional heat treatments which can, to a certain extent, alter the microstructure stress and partially relieve it. This would decrease the inhomogeneity of the magnetocaloric response in case it arises from microstructural stress. Possible additional steps include changing the heat treatment protocol and/or changing the melting procedure, such as induction melting. These could, however, alter the outcome of the synthesis and would therefore require additional work due to their impact on the outcome of the synthesis and the possibility of providing different final results.

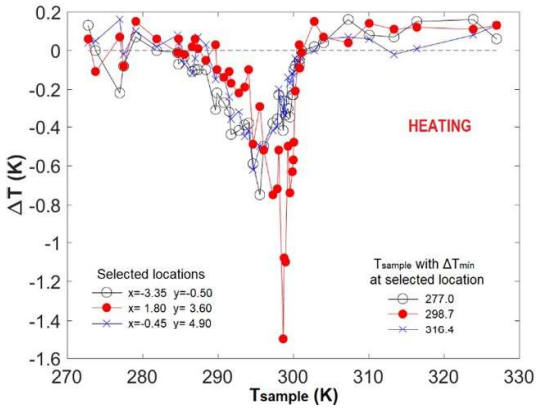

Figure 9. ΔT vs T_{sample} on heating for selected locations of the sample surface. The locations were determined by selecting three T_{sample} values of interest and finding the map coordinates for which the minimum value of ΔT occurred.

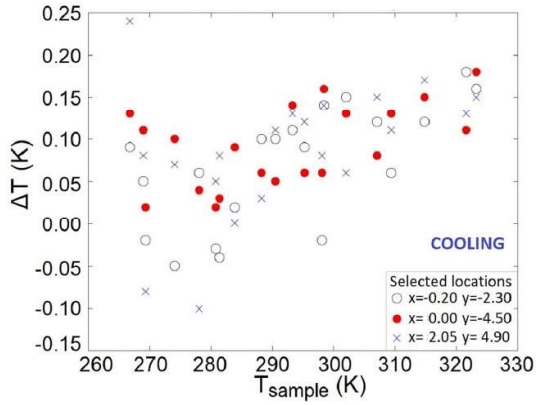

Figure 10. ΔT vs T_{sample} for the same locations from figure 8, now on cooling.

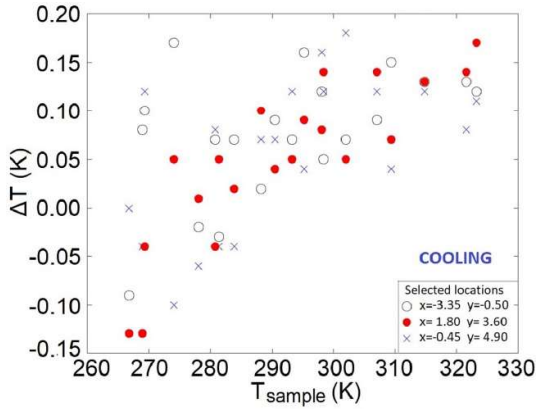

Figure 11. ΔT vs T_{sample} for the same locations from figure 9, now on cooling.

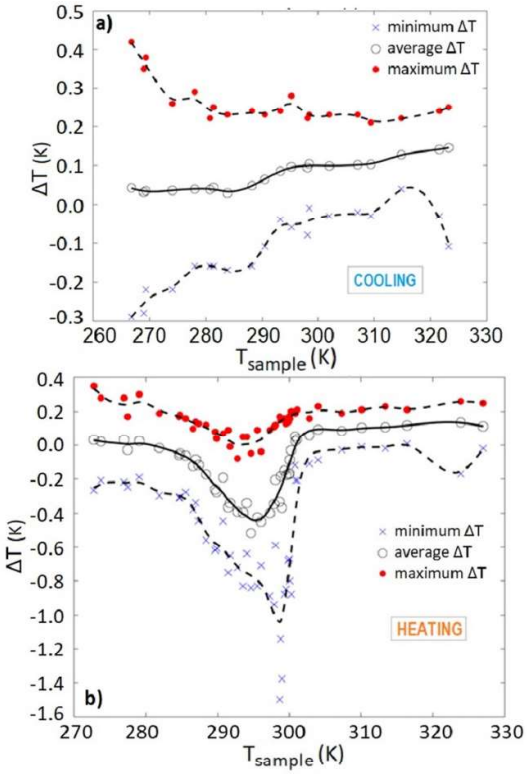

Figure 12. Plot of the temperature variation after and before the magnetic field was applied for the sample locations exhibiting the maximum and the minimum values of the MCE for each T_{sample} value on cooling (a) and heating (b). Average temperature variation is offered for comparison.

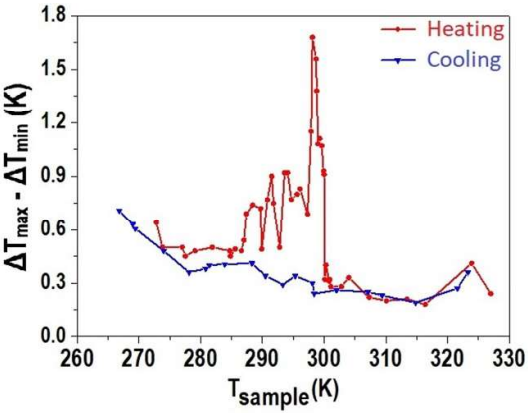

Figure 13. Difference between the maximum and minimum values of the magnetocaloric effect (identified in distinct positions (pixel) on the sample) at each considered sample temperature.

4. Conclusion

This work demonstrated the ability to discriminate the microscopic behavior of the MCE in a bulk FSMA sample. In each portion of the sample within a scale of about 80 μm the MCE manifests in an individual manner, which does not necessarily match the behavior of the average of all micrometric portions composing the entire sample. We have thus enabled the assessment of minority behaviors, which cannot be discriminated through macroscopic measurements. Knowledge on minority behaviors may be of utmost importance on several instances, from sample preparation to device performance evaluation.

Mapping of the MCE across all the probed area of the sample presented the relative contribution of each microscopic portion of the sample, discerning minority behaviors of the effect, especially for temperatures in the vicinity of the transformation on the heating process. The behavior might arise from localized microstructural stress since compositional heterogeneity was found to be below experimental uncertainty.

The wider temperature variation resulting from the MCE manifestation does not occur at the same temperature for each microscopic region of the sample. This indicates that the structural transformation does not occur at the same temperature for said regions. We are thus also able to discriminate the behavior of the transformation at the microscale. In summary, the study innovates by constructing quantitative MCE maps to evaluate minority behaviors in the MCE in contrast with the average behavior of the effect.

Data availability statement

All data that support the findings of this study are included within the article (and any supplementary files).

Acknowledgments

This work was developed within the scope of the projects CICECO-Aveiro Institute of Materials, UIDB/50011/2020, UIDP/50011/2020 & LA/P/0006/2020, financed by National funds through the FCT/MEC (PIDDAC) and NANOCERAMPROBE POCI-01-0145-FEDER-032117, funded by National funds through the FCT/MECTES (FEDER-PT2020).

Tiago Santos acknowledges the post-doctoral grant under the project BPD—SGH/CICECO-UA/137B-02/2019, within the scope of the R&D Co-Promotion Project SGH—SMART GREEN HOMES (POCI-01-0247-FEDER-007678) and the support of CICECO-Aveiro Institute of Materials, FCT Ref. UID/CTM/50011/2019, financed by National funds through the FCT /MCTES.

ORCID iD

Maria J Pereira https://orcid.org/0000-0002-7369-5881

References

[1] Pollock H M and Hammiche A 2001 *J. Phys. D: Appl. Phys.* **34** R23–53
[2] Tishin A M and Spichkin Y I 2014 *Int. J. Refrig.* **37** 223
[3] Tishin A M, Pichkin Y I, Zverev V I and Egolf P W 2016 *Int. J. Refrig.* **68** 177–86
[4] Cugini F and Solzi M 2020 *J. Appl. Phys.* **127** 123901
[5] Li Z, Dong S, Li Z, Yang B, Liu F, Sánchez-Valdés C F, Sánchez Llamazares J L, Zhang Y, Esling C, Zhao X and Zuo L 2019 *Scr. Mater.* **159** 113–8
[6] Li Z *et al* 2019 *Adv. Electron. Mater.* **5** 1800845
[7] Cugini F, Porcari G and Solzi M 2014 *Rev. Sci. Instrum.* **85** 074902
[8] Kamantsev A P *et al* 2017 *J. Magn. Magn. Mater.* **440** 70–73
[9] Hirayama Y, Iguchi R, Miao X-F, Hono K and Uchida K-I 2017 *Appl. Phys. Lett.* **111** 163901
[10] Christensen D V, Bjørk R, Nielsen K K, Bahl C R H, Smith A and Clausen S 2010 *J. Appl. Phys.* **108** 063913
[11] Wang K, Ouyang Y, Shen Y, Zhang Y, Zhang M and Liu J 2021 *J. Mater. Sci.* **56** 2332–40
[12] Zavareh M G, Mejía C S, Nayak A K, Skourski Y, Wosnitza J, Felser C and Nicklas M 2015 *Appl. Phys. Lett.* **106** 071904
[13] Cugini F, Orsi D, Brück E and Solzi M 2018 *Appl. Phys. Lett.* **113** 232405
[14] Modak R, Iguchi R, Sepehri-Amin H, Miura A and Uchida K-I 2020 *AIP Adv.* **10** 065005
[15] Pereira M J, Santos T, Correia R, Amaral J S, Amaral V S, Fabbrici S and Albertini F 2021 *J. Magn. Magn. Mater.* **538** 168283
[16] Fabbrici S *et al* 2011 *Acta Mater.* **59** 412–9
[17] Porcari G, Cugini F, Fabbrici S, Pernechele C, Albertini F, Buzzi M, Mangia M and Solzi M 2012 *Phys. Rev.* B **86** 104432
[18] (Available at: www.youtube.com/watch?v=Q1pquw_2cIE)
[19] (Available at: www.youtube.com/watch?v=WmZBCmeCnIA)
[20] Skokov K P *et al* 2010 *Phys. Rev.* B **81** 214406